THE JOURNAL OF BIOLOGICAL CHEMISTRY
Vol. 280, No. 4, Issue of January 28, pp. 2962–2971, 2005
Printed in U.S.A.

Allele-dependent Similarity between Viral and Self-peptide Presentation by HLA-B27 Subtypes*

Received for publication, September 20, 2004, and in revised form, October 26, 2004
Published, JBC Papers in Press, November 10, 2004, DOI 10.1074/jbc.M410807200

Maria Teresa Fiorillo‡§, Christine Rückert§¶, Martin Hülsmeyer§‖, Rosa Sorrentino‡, Wolfram Saenger‖, Andreas Ziegler¶, and Barbara Uchanska-Ziegler¶‡‡**

From the ‡Dipartimento di Biologia Cellulare e dello Sviluppo, Università di Roma "La Sapienza," via dei Sardi 70, 00185 Roma, Italy, the ¶Institut für Immungenetik, Charité-Universitätsmedizin Berlin, Campus Virchow-Klinikum, Humboldt-Universität zu Berlin, Spandauer Damm 130, 14050 Berlin, Germany, and the ‖Institut für Chemie/Kristallographie, Freie Universität Berlin, Takustrasse 6, 14195 Berlin, Germany

Molecular mimicry is discussed as a possible mechanism that may contribute to the development of autoimmune diseases. It could also be involved in the differential association of the human major histocompatibility subtypes *HLA-B*2705* and *HLA-B*2709* with ankylosing spondylitis. These two subtypes differ only in residue 116 of the heavy chain (Asp in B*2705 and His in B*2709), but the reason for the differential disease association is not understood. Using x-ray crystallography, we show here that the viral peptide pLMP2 (RRRWRRLTV, derived from latent membrane protein 2 (residues 236–244) of Epstein-Barr virus) is presented by the B*2705 and B*2709 molecules in two drastically deviating conformations. Extensive structural similarity between pLMP2 and the self-peptide pVIPR (RRKWRRWHL, derived from vasoactive intestinal peptide type 1 receptor (residues 400–408)) is observed only when the peptides are presented by B*2705 because of a salt bridge between Arg^{5} of both peptides and the subtype-specific heavy chain residue Asp^{116}. Combined with functional studies using pLMP2/pVIPR-cross-reactive cytotoxic T cell lines and clones, together with target cells presenting these peptides or a modified peptide analogue, our results reveal that a pathogen-derived peptide can exhibit major histocompatibility complex class I subtype-dependent, drastically distinct binding modes. Furthermore, the results demonstrate that molecular mimicry between pLMP2 and pVIPR in the HLA-B27 context is an allele-dependent property.

Not all *HLA-B27* subtypes are equally associated with the autoimmune disease ankylosing spondylitis (AS).[1] The frequent, prototypical subtype *B*2705* is AS-associated, independent of ethnic origin, whereas *B*2706* and *B*2709*, which exhibit geographically restricted distribution, are not (1). The products of the *B*2705* and *B*2709* alleles differ only in residue 116 of the HLA-B27 heavy chain (HC; Asp in B*2705 and His in B*2709) (2). This residue is located at the floor of the peptide-binding groove, forms part of the F-pocket, and is buried upon binding of a peptide. Despite the close structural similarities, the subtypes give rise to distinct repertoires of bound peptides (3) and cytotoxic T lymphocytes (CTL) (4). *B*2705*-positive but not *B*2709*-positive individuals possess CTL that recognize the HLA-B27-bound self-peptide pVIPR (RRKWRRWHL). pVIPR is derived from vasoactive intestinal peptide type 1 receptor (residues 400–408) and is presented by B*2709 molecules in the common canonical conformation, whereas B*2705 presents the peptide in an unusual dual binding mode (5).

pVIPR exhibits sequence homology with the peptide pLMP2 (RRRWRRLTV), derived from latent membrane protein 2 (residues 236–244) of Epstein-Barr virus (EBV). The existence of CTL reacting with both peptides in the context of B*2705 suggests a relationship between infection with EBV and an expansion of the pool of pLMP2/pVIPR-cross-reactive CTL (4). However, a direct correlation between EBV infection and AS pathogenesis has not been established. Molecular mimicry (6–9), *i.e.* similarity in overall shape as well as charge distribution for an interaction surface (9), has been invoked as an explanation for the association of *HLA-B27* and spondyloarthropathies (10–12), but its existence has yet to be proven (13, 14). A principal difficulty is related to the fact that a host-derived epitope is expected to share antigenic but not necessarily also extensive sequence homology with a foreign antigen (15).

We have now determined the structures of both HLA-B27 subtypes in complex with pLMP2 and compare them here with the corresponding pVIPR complexes. Together with functional data, this comparison suggests that structural similarity and CTL cross-reactivity between pLMP2 and pVIPR in the context of HLA-B27 antigens are allele-dependent properties.

EXPERIMENTAL PROCEDURES

HLA-B27-positive Donors, CTL Lines, and Clones—Seven patients with AS (with the exception of one *B*2702*-positive individual, all typed as *B*2705*) and two healthy individuals (one *B*2705*-positive and one *B*2709*-positive) were enrolled for this study (see Tables III, IV, and V). *HLA-B27* typing and generation of pLMP2- and pVIPR-specific CTL lines were carried out as described (4). The CTL line MP VPAC7 was cloned by limiting dilution at 0.5–1 cell/well in 96-well U-bottom microplates in the presence of phytohemagglutinin (0.5 μg/ml), 3×10^4 allogeneic γ-irradiated peripheral blood mononuclear cells, and 20 units/ml recombinant interleukin-2 (Roche Applied Science). After 12 days, the growing cells were restimulated with pVIPR-pulsed, γ-irradi-

* This work was financially supported by Deutsche Forschungsgemeinschaft Grant SFB 449, TP B5,B6; Sonnenfeld-Stiftung; COFIN 2001; and Istituto Pasteur Fondazione Cenci-Bolognetti. The costs of publication of this article were defrayed in part by the payment of page charges. This article must therefore be hereby marked "*advertisement*" in accordance with 18 U.S.C. Section 1734 solely to indicate this fact.

The atomic coordinates and structure factors (code 1uxs and 1uxw) have been deposited in the Protein Data Bank, Research Collaboratory for Structural Bioinformatics, Rutgers University, New Brunswick, NJ (http://www.rcsb.org/).

§ These authors contributed equally to this work.

** To whom correspondence may be addressed. Tel.: 49-30-8385-3412; Fax: 49-30-8385-6702; E-mail: saenger@chemie.fu-berlin.de.

‡‡ To whom correspondence may be addressed. Tel.: 49-30-4505-53517; Fax: 49-30-4505-53953; E-mail: barbara.uchanska-ziegler@charite.de.

[1] The abbreviations used are: AS, ankylosing spondylitis; EBV, Epstein-Barr virus; HLA, human leukocyte antigen; MHC, major histocompatibility complex; HC, heavy chain; CTL, cytotoxic T lymphocyte(s); HIV, human immunodeficiency virus; TCR, T cell receptor.

TABLE I
Data collection and refinement statistics

	HLA-B*2705·pLMP2	HLA-B*2709·pLMP2
Data collection		
Space group	$P2_1$	$P2_1$
Unit cell (Å, Å, Å; °)	51.1, 82.3, 65.9; 109.3	50.9, 82.6, 62.8; 104.4
Resolution (Å)[a]	40.0–1.55 (1.61–1.55)	40.0–1.72 (1.78–1.72)
Unique reflections	74,438 (7225)	53,353 (5036)
Completeness (%)[a]	99.4 (97.0)	99.4 (96.0)
I/σ^a	21.0 (4.1)	20.2 (3.7)
$R_{sym}{}^{a,b}$	0.051 (0.246)	0.045 (0.262)
Refinement		
Nonhydrogen atoms	3992	3876
$R_{cryst}{}^{a,c}$	0.142 (0.179)	0.154 (0.183)
$R_{free}{}^{a,d}$	0.177 (0.202)	0.190 (0.224)
Heavy chain, no. of atoms/average B factor (Å^2)	2301/20.0	2298/12.85
β_2-Microglobulin, no. of atoms/average B factor (Å^2)	855/23.0	860/17.9
Peptide, no. of atoms/average B factor (Å^2)	102/19.6	92/10.3
Water, no. of molecules/average B factor (Å^2)	710/38.7	596/33.7
Glycerol, no. of atoms/average B factor (Å^2)	24/37.4	30/21.5
Estimated overall coordinate error (Å)[e]		
Root mean square deviation from ideal geometry		
Bond length (Å)	0.015	0.015
Bond angles (°)	1.5	1.6

[a] The values in parentheses refer to the highest resolution shell.
[b] $R_{sym} = \Sigma_h \Sigma_i |I_{h,i} - \langle I_h \rangle| / \Sigma_h \Sigma_i I_{h,i}$.
[c] $R_{cryst} = \Sigma_h |F_o - F_c| / \Sigma F_o$ (working set, no σ cut-off applied).
[d] R_{free} is the same as R_{cryst}, but calculated on 5% of the data excluded from refinement.
[e] Estimated overall coordinate error based on R_{free} as calculated by Refmac 5.1.1999.

ated autologous B-LCL and further expanded in the presence of recombinant interleukin-2 (20–50 units/ml).

Cytotoxicity Assays—Cytolytic activity of pLMP2-responsive (RRRWRRLTV), pVIPR-responsive (RRKWRRWHL), and pVIPR-pArg^3-responsive (RRRWRRWHL) CTL lines and clones was assessed according to the standard ^{51}Cr release procedure (4). Target cells (B*2705 or B*2709 T2 transfectants) were incubated overnight with the pLMP2 or pVIPR peptides at 70 μM or at lower concentrations (see "Results" and Fig. 4 for details) or in medium alone. One day later, the cells were labeled with sodium chromate and extensively washed before being mixed with effector T cells at 3×10^3 target cells/well.

Analysis of TCR Gene Usage—Total RNA was extracted from 2×10^5 T cells, and cDNA was synthesized using oligo(dT) primer and SuperScript™ II RNase H$^-$ Reverse Transcriptase (Invitrogen) according to the manufacturer's instructions. For the analysis of TCR α chain usage, cDNA was amplified using primers and PCR conditions as already described (16). Additional oligonucleotides for Vα families 18–29 were designed as detailed previously (17). PCR products were loaded on a 1.5% agarose gel stained with ethidium bromide. Specific DNA bands were cut from the gel and purified using a gel band purification kit (Amersham Biosciences). Direct sequencing was performed using an internal primer upstream of the TCR Cα reverse primer.

Protein Preparation and Structure Determination—The peptide pLMP2 was purified by high pressure liquid chromatography (Alta Bioscience), and HLA-B27·peptide complexes were produced as described (5). Purified complexes (15–20 mg/ml in 20 mM Tris/HCl, 150 mM NaCl, 0.01% sodium azide, pH 7.5) were used for crystallization using hanging drop vapor diffusion and streak-seeding. Crystals suitable for x-ray diffraction experiments were grown in drops made of 1.5 μl of protein solution and 1.5 μl of precipitant solution (for B*2705, 15% polyethylene glycol 8000, 0.1 M Tris/HCl, pH 7.5, and for B*2709, 21% polyethylene glycol 8000, 0.1 M Tris/HCl, pH 8.5). Using glycerol as cryoprotectant, data sets were obtained from cryo-cooled (100 K) crystals at the BL2 beam line of BESSY-II. The data were processed with the HKL package (see Table I) (18).

The structure of B*2709·pLMP2 was determined by molecular replacement using peptide-stripped B*2709·m9 (Protein Data Bank code 1k5n) as a search model and the program Molrep (19). After rigid body refinement using Refmac (20), the initial model was subjected to simulated annealing and energy minimization using CNS (21) to remove model bias. Further refinement was carried out by iterative cycles of manual rebuilding using O (22) and restrained maximum-likelihood with Refmac comprising B-factor adjustment. Water molecules were included with *ARP/wARP* (23). After translation, libration, screw rotation refinement (24), the R factor converged at 0.154 (R_{free} = 0.190). As the two HLA-B27·pLMP2 complexes crystallized isomorphously, initial phases for B*2705·pLMP2 were calculated from peptide-stripped B*2709·pLMP2 with His^{116} replaced by alanine. This initial model was subjected to rigid body refinement, simulated annealing, and energy minimization using CNS, improved by manual intervention using O and water molecule inclusion as described for the B*2709-data processing. Because of the higher resolution of B*2705·pLMP2, restrained maximum-likelihood refinement (Refmac) included anisotropic B-factor refinement. Evaluation of the atomic displacement parameters by Parvati (25) provided the expected statistical distribution of 0.5 ± 0.17 for all atoms of the structure. Both structures were validated with Whatcheck (26), and the statistics are compiled in Table I. The figures were generated using Delphi (27), Povray (www.povray.org), Molscript (28), Rastop (www.geneinfinity.org/rastop/), MSMS (29), and Raster3D (30) together with a graphical interface (Moldraw) developed by N. Sträter (Institut für Kristallographie, Freie Universität Berlin).[2]

The atomic coordinates and structure amplitudes have been deposited in the Protein Data Bank under accession codes 1uxs (B*2705·pLMP2) and 1uxw (B*2709·pLMP2).

RESULTS

Structural Features of pLMP2 in Complex with HLA-B27 Subtypes—The B*2705·pLMP2 and B*2709·pLMP2 complexes crystallized isomorphously in space group $P2_1$ (Table I). Both show the typical MHC class I topography (31) (Fig. 1, *a–c*) and were refined at high resolution: 1.55 Å for B*2705·pLMP2 and 1.72 Å for B*2709·pLMP2. The HLA-B27 HC and β_2-microglobulin are highly similar in the two subtypes (except for the D116H exchange) with a Cα root mean square deviation of only 0.2 Å. For each complex, the peptide could be modeled unambiguously to the electron density (Fig. 1, *d* and *e*). When complexed to B*2709, pLMP2 is bound in the conventional p4α conformation (main chain φ/ψ torsion angles in α-helical conformation at p4), with the solvent-exposed pArg^5 side chain pointing away from the binding groove (Fig. 1*b*) (5). In contrast, pLMP2 displays the drastically different p6α conformation (main chain φ/ψ torsion angles in α-helical conformation at p6) when bound to B*2705 (Fig. 1*a*), with the side chain of pArg^5 pointing toward the interior of the binding groove, where it forms a salt bridge with HC Asp^{116} (5). These subtype-dependent pArg^5 orientations force the middle portion (residues p4–p7) of the peptide backbones and the corresponding amino acid side chains into grossly different conformations in the two

[2] N. Sträter, unpublished program.

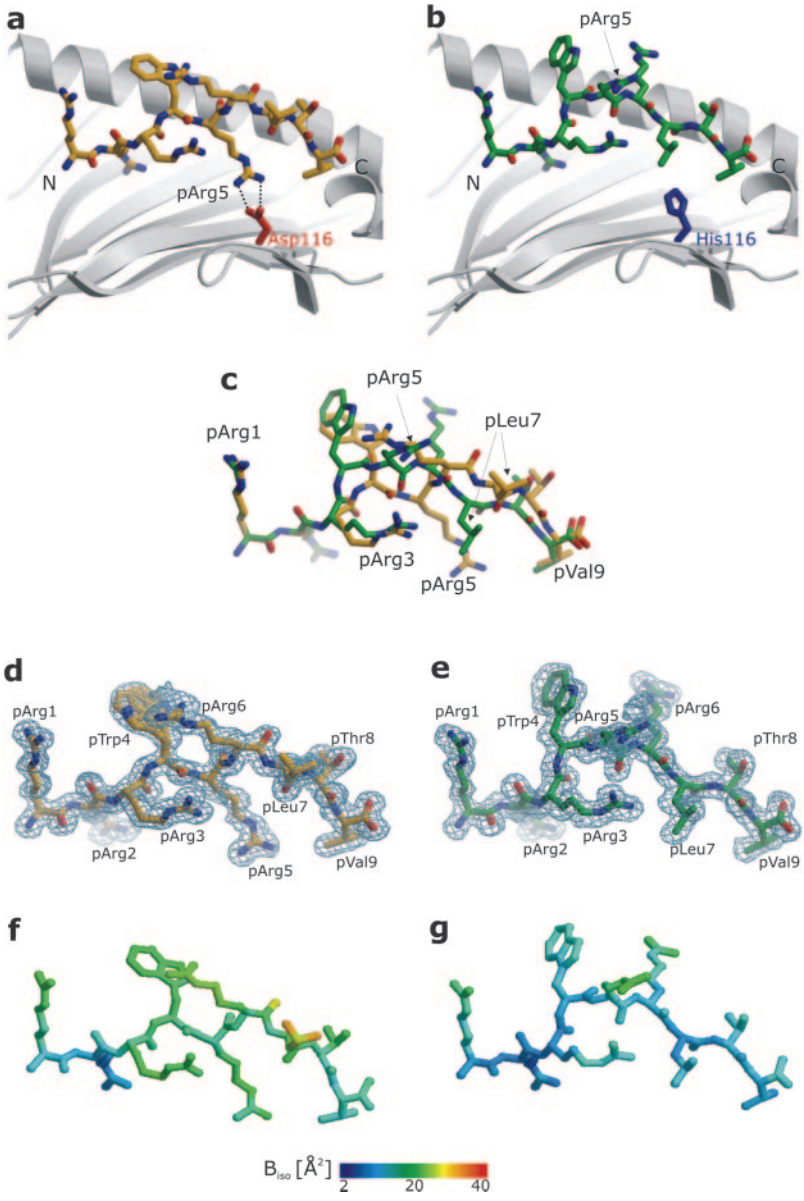

FIG. 1. **pLMP2 topographies, electron densities, and B factors when bound to B*2705 and B*2709.** *a* and *b*, conformation of pLMP2 in B*2705 and B*2709, viewed from the side of the α2-helix together with a ribbon representation of the α1-helix and the floor (β-sheet) of the binding groove. The subtype-specific residue 116 is indicated (Asp^{116}, *red*; His^{116}, *blue*), with the bidentate salt bridge to Asp^{116} shown as *dotted lines*. In *b*, $pArg^5$ points toward the viewer. *c*, superimposition of pLMP2 in B*2705 and B*2709, viewed as in *a* and *b*, showing that the peptide conformations in the two subtypes differ drastically from $pTrp^4$ to $pThr^8$. *d* and *e*, final $2F_o - F_c$ electron density contoured at the 1 σ level of pLMP2 conformations in B*2705 (*d*) and B*2709 (*e*). Water molecules are omitted for clarity from the representations in *a*–*e*. *f* and *g*, pLMP2 bound by B*2705 (*f*) and B*2709 (*g*), color-coded by isotropic B factor. A quantitative comparison is made difficult by the refinement strategies employed (anisotropic for B*2705 and isotropic for B*2709).

subtypes (Fig. 1*c*). Because these regions of the two complexes do not participate in extensive crystal contacts, the observed conformational differences must be a direct consequence of the D116H polymorphism.

The N-terminal pLMP2 residues $pArg^1$, $pArg^2$, and $pArg^3$ occupy identical positions in both subtypes (Fig. 1*c* and Table II). Both subtypes exhibit also closely related interactions between HC atoms and C-terminal peptide residues $pThr^8$ and $pVal^9$. In B*2709, however, p8 and p9 are located slightly deeper in the binding groove than in B*2705 (Fig. 1, *a*–*c*), possibly as a consequence of altered p4–p7 conformations. To account for these changes, the binding groove residues in contact with $pThr^8$ and $pVal^9$ (Table II) exhibit small side chain variations.

$pTrp^4$ is the first pLMP2 residue with substantially different positioning in the two subtypes (Fig. 1, *a*–*e*, and Table II). In p4α conformation found in complex with B*2709, the $pTrp^4$, $pArg^5$, and $pArg^6$ side chains are fully solvent-exposed, with few HC contacts, whereas $pLeu^7$ projects into the E-pocket (Fig. 1, *b*, *c*, and *e*, and Table II). A very different situation is found in the p6α conformation seen in B*2705 (Fig. 1, *a*, *c*, and *d*). Here, the $pTrp^4$ side chain is packed against the α1-helix, and $pArg^5$ forms a salt bridge with Asp^{116} that leads to deeper insertion of the middle section of the peptide into the binding groove (Fig. 1*a* and Table II). At $pArg^6$, the peptide backbone bends upward (associated with the p6α conformation), so that the side chain can engage in van der Waals' contact with $pTrp^4$ (Table II). Finally, $pLeu^7$ is solvent-exposed in B*2705, and its side chain exhibits the highest flexibility of all pLMP2 residues in either conformation as shown by temperature (B) factors (Fig. 1, *f* and *g*, and Table I). A comparison of the B factors of the peptide reveals that pLMP2 is more flexibly bound in B*2705 despite the anchoring of its middle through the $pArg^5$-Asp^{116} interaction. This differential peptide flexibility is most likely a consequence of a network of solvent molecules that is tighter in B*2709 than in B*2705, where the hydrophobic section of the $pArg^5$ side chain prevents its formation.

*Structural Comparison of pLMP2 and pVIPR in Complexes with B*2705 and B*2709*—The four complexes of B*2705 and B*2709 with pLMP2 and pVIPR, respectively, crystallized isomorphously (Ref. 5 and Table I), indicating that the same crystallographic restraints (intermolecular interactions associated with crystal packing) apply to all of them. Comparison of pVIPR complexed with B*2705 and with B*2709 has already been carried out, with the dual p4α/p6α conformation found in B*2705 but not in B*2709, where only p4α occurs (5). Therefore, if molecular mimicry were to play a role in the

TABLE II

*Comparison of pLMP2 peptide coordination in the B*2705 and B*2709 subtypes*

Only direct intrapeptide contacts and contacts between pLMP2 and HC residues are included, and solvent-mediated interactions are omitted. van der Waals' contacts are not given explicitly for each amino acid. In the B*2705 subtype, $pTrp^4$ and Asp^{116} occur in alternative conformations. Only one of the equally occupied $pTrp^4$ conformations and the higher occupied Asp^{116} conformation ($q = 0.75$) are shown and discussed in the text.

	B*2705:pLMP2				B*2709:pLMP2			
Peptide residue	**Atom**	**Contact residue**	**Distance [Å]**	**Interaction**	**Atom**	**Contact residue**	**Distance [Å]**	**Interaction**
pArg1 pArg2 pArg3	Contacts formed by pArg1, pArg2, and pArg3 are very similar in both subtypes							
pTrp4	*solvent-exposed*				*solvent-exposed*			
	pTrp4	$pArg6^{GuaA}$ $Ile66^{B}$	3.3-3.5 3.5-3.7	v.d.Waals v.d.Waals	No direct contacts to peptide or HC residues			
pArg5	*Buried*				*solvent-exposed*			
	$pArg5^{NH1}$	$Asp116^{OD1C}$	3.13	salt bridge	No direct contacts to peptide or HC residues			
	$pArg5^{NH2}$	$Asp116^{OD2C}$	2.98	salt bridge				
pArg6	*solvent-exposed*				*solvent-exposed*			
	$pArg6^{Gua}$	$pTrp4^{A}$	3.3-3.5	v.d.Waals	$pArg6^{NH1}$	$Glu72^{OE1B}$	3.12	salt bridge
					pArg6	$Ala69^{B}$	3.6	v.d.Waals
pLeu7	*solvent-exposed*				*Buried*			
	pLeu7	$Val152^{D}$	~3.5	v.d.Waals	pLeu7	$Trp147^{D}$	3.6-3.7	v.d.Waals
					pLeu7	$Val152^{D}$	3.6-3.7	v.d.Waals
pThr8 pVal9	Contacts formed by pThr8 and pVal9 are very similar in both subtypes							

[a] Intrapeptide contact.
[b] Helix α1.
[c] β-Sheet floor.
[d] Helix α2.

context of the pLMP2/pVIPR structures, as suggested by CTL cross-reactivity (4), a comparison of side chain orientations (Fig. 2) and surface properties (Fig. 3) between the two pLMP2 complexes and the two pVIPR complexes should provide a structure-based explanation.

The structures of the two peptides in B*2705 immediately reveal that pLMP2 (Fig. 3*a*) is much more similar to pVIPR-p6α (Cα root mean square deviation of 0.3 Å; Fig. 3*c*) than to pVIPR-p4α (Cα root mean square deviation of 1.6 Å; Fig. 3*d*). $pArg^1$ as well as the anchor residues $pArg^2$ and $pVal^9$/$pLeu^9$ occupy virtually identical positions (Fig. 2, *a* and *b*). As expected from the peptide sequences, the similarity of pVIPR and pLMP2 is most pronounced in the N-terminal half, extending to $pArg^6$. In addition to the amino acid exchange at p7, the solvent-exposed $pHis^8$ in pVIPR and $pThr^8$ in pLMP2 lead to a marked topographical change near the peptide C termini (Figs. 2, *a* and *b*, and 3, *a* and *c*). The similarity between B*2705·pLMP2 (p6α binding mode) and B*2705·pVIPR-p6α extends beyond conformational (Figs. 2, *a* and *b*, and 3, *a* and *c*) to electrostatic properties of their surfaces (Fig. 3, *e* and *g*), particularly in the N-terminal halves of the peptides. In contrast, pLMP2 and pVIPR-p4α in B*2705 are less equivalent at residues p4–p8 (Figs. 2, *c* and *d*, and 3, *a* and *d*). The electrostatic surfaces of the two complexes in p4α/p6α conformation diverge considerably as well (Fig. 3, *e* and *h*). It seems therefore plausible to conclude that pLMP2/pVIPR CTL cross-reactivity is more likely to occur when pVIPR is displayed in p6α than in p4α conformation.

Surprisingly, the p4α conformations of the two peptides found in B*2709 differ much more (Cα root mean square deviation of 0.9 Å; Figs. 2, *e* and *f*, and 3, *b*, *d*, *f*, and *h*) than the two p6α conformations in B*2705 (Figs. 2, *a* and *b*, and 3, *a*, *c*, *e*, and *g*). Again, residues p1, p2, p4, and p9 show negligible variations, and $pLys^3$ (pVIPR) also occupies a similar position as $pArg^3$ (pLMP2). However, the side chain guanidinium moieties of both $pArg^5$ residues are solvent-exposed and point to opposite directions (Figs. 2, *e* and *f*, and 3, *b* and *d*), whereas those in p6α conformation (Figs. 2, *a* and *b*, and 3, *a* and *c*) are buried. $pArg^6$ displays a substantial difference as well; in pLMP2, this side chain is completely solvent-accessible with only a few contacts to the α1-helix, whereas it wedges between the peptide backbone and the α1-helix in the complex with pVIPR (5). The Cα atoms of $pArg^6$ deviate by 2.3 Å, and the disparity between the guanidinium groups is even larger. Although more similarly positioned, the p7-Cα atoms still differ by 1.6 Å. The side chain of $pTrp^7$ (pVIPR) occupies the front part of the large E-pocket, an impossible location for $pLeu^7$ (pLMP2) because of steric hindrance exerted by the large $pArg^3$ located in the neighboring D-pocket. As a consequence, $pLeu^7$ occupies the back part of the E-pocket, toward the peptide C terminus, is inserted deeper than $pTrp^7$ in pVIPR, and is shifted toward the α1-helix. The peptides deviate only by 1.1 Å at Cα of p8, but the

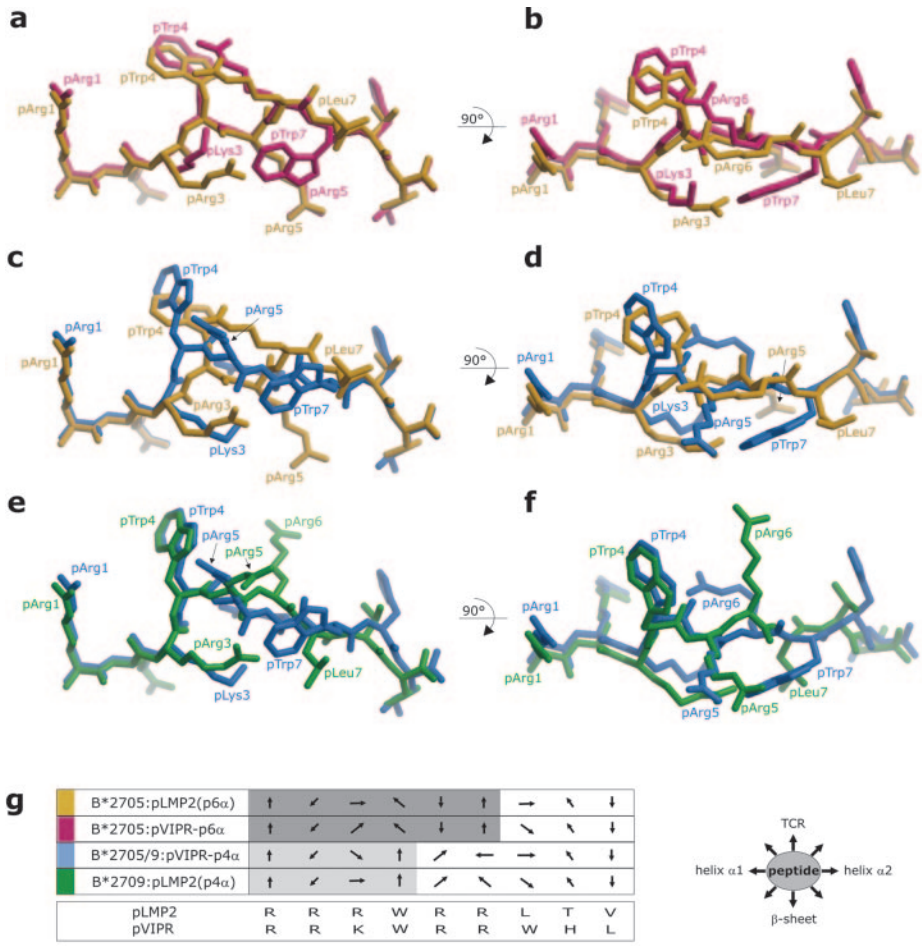

FIG. 2. **Comparison of pVIPR and pLMP2 as presented by B*2705 and B*2709.** Superimpositions in two views rotated 90° with respect to each other; selected amino acids are indicated. *a* and *b*, superimposition of pLMP2 (*yellow*) and pVIPR (*magenta*), both in p6α binding mode, as presented by B*2705 molecules, viewed from the side (*a*, same view as in Fig. 1*a*) or the top (*b*). *c* and *d*, superimposition of pLMP2 (*yellow*, p6α conformation) and pVIPR-p4α (*blue*) as presented by B*2705 molecules, viewed from the side (*c*) or the top (*d*). *e* and *f*, superimposition of pLMP2 (*green*) and pVIPR (*blue*), both in p4α binding mode, as presented by B*2709 molecules, viewed from the side (*e*) or the top (*f*). *g*, *left panel*, schematic description of side chain orientations when looking from the N to the C termini of pLMP2, pVIPR-p6α, and pVIPR-p4α in the two HLA-B27 subtypes. The *shaded areas* indicate structural similarity between the two peptides as presented by B*2705 (*dark gray*) and B*2709 (*light gray*). *Right panel*, floor of peptide binding groove indicated by *β-sheet*, and binding region for TCR indicated by *TCR*.

side chains display different shapes (Fig. 3, *b* and *d*) and electrostatic potentials (Fig. 3, *f* and *h*). These similarities and differences suggest that pLMP2/pVIPR-cross-reactive CTL from B*2709 individuals are likely to recognize predominantly epitopes formed by p1–p4 (Fig. 2*g*) and the adjacent residues of the binding groove.

Peptide- and Subtype-dependent CTL Recognition—We have previously shown that autoreactive CTL lines from individuals typing as *B*2705* are frequently observed in patients with AS but occur in reduced numbers in healthy individuals. Such CTL are only rarely found in *B*2709* individuals, and pLMP2/pVIPR-cross-reactive CTL are infrequently observed among pLMP2-reactive CTL from either subtype (4). To better understand the nature of this cross-reactivity, we have now carried out more extensive studies with CTL, also including CTL clones as well as a hybrid peptide (pVIPR-pArg^3) in which pLys^3 (from pVIPR) is replaced by pArg^3 (as in pLMP2; Tables III, IV, and V). This exchange was thought to influence epitope recognition by cross-reactive CTL. The ability of pVIPR-pArg^3 to stabilize both B*2705 and B*2709 molecules has been evaluated as already described for pVIPR and pLMP2 (Ref. 4 and data not shown).

pLMP2-stimulated CTL from either *HLA-B27* subtype detect this peptide also in the context of the other subtype (Table III), implying that structurally similar regions around p1–p3 or p8 provide the epitope(s) (Fig. 1*c*). About one-sixth of these CTL cross-react with pVIPR at high peptide concentration (70 μM), irrespective of the subtype presenting this peptide. Furthermore, about 25% of the pVIPR-stimulated CTL from *B*2705* individuals cross-react with pLMP2 and recognize both peptides also in the B*2709 context. In addition, all pVIPR-stimulated CTL from *B*2705* individuals that cross-react with pLMP2 recognize both peptides also in the B*2709 subtype (Table IV). Four pLMP2/pVIPR-cross-reactive CTL lines, two from a *B*2709*-positive individual (Ci) and two from a *B*2705*-positive AS patient (MP), were also tested at lower peptide concentrations (Fig. 4). It is evident that when B*2709 presents the two peptides, the dose-response curves have a similar profile (Fig. 4, *b*, *d*, *f*, and *h*). In contrast, when it is B*2705 that displays the two peptides, the CTL of the patient show a strikingly higher preference for pLMP2 (Fig. 4, *e* and *g*), even though they derive from a stimulation with pVIPR. In case of B*2705, the difference between the two peptides was found to be about 100-fold.

The reactivity against pVIPR and pLMP2 either in the B*2705 or in the B*2709 context has been tested also with several clones derived from the CTL line MP VPAC7. Representative dose-response curves of one CTL clone are shown using also lower peptide concentrations (Fig. 4, *i* and *j*). The profiles are similar to those obtained with the parental CTL line; in particular, we found that the clonal reactivities were always much stronger against pLMP2, although this peptide was not employed for the initial stimulations of the CTL. TCR gene usage was assessed for 17 clones derived from MP VPAC7. The results obtained with clone 8 (Fig. 4, *i* and *j*) are representative for the others. The same TCR-AV14 chain, CDR3 motif (DRDDKI), and J segment (AJ9S4) were found (Fig. 4*k*). A higher degree of variability was found for TCR β-chains, but TCRBV1BJ2S1 chains were predominant among the MP VPAC7-derived clones.

Experiments with the pVIPR-pArg^3 peptide show that even a conservative amino acid replacement in the N-terminal half of

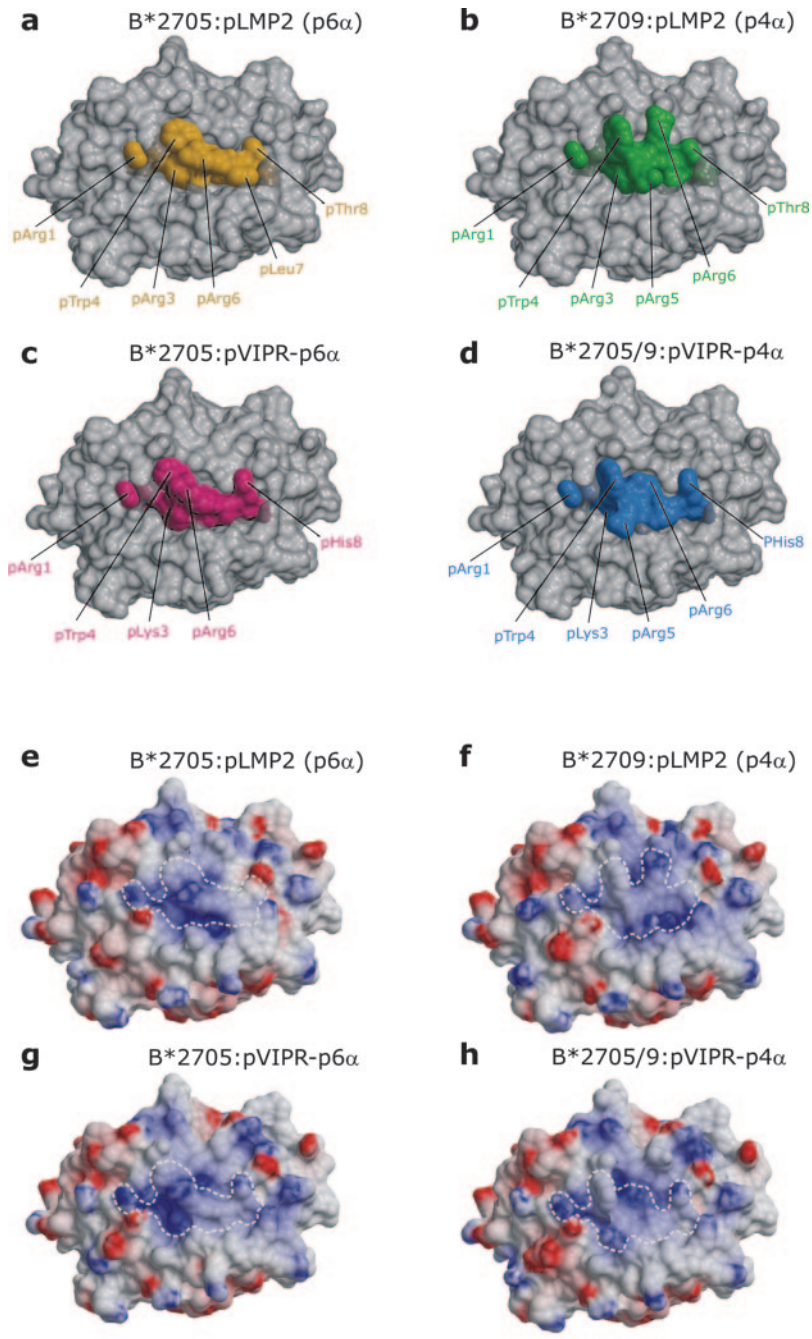

FIG. 3. **Molecular surfaces of pLMP2 and pVIPR as presented by B*2705 and B*2709.** Molecular surface representations of B*2705 (*a*, *c*, *e*, and *g*) and B*2709 (*b*, *d*, *f*, and *h*) complexed with pLMP2 or pVIPR, as viewed by an approaching TCR; color-coding is as in Figs. 1 and 2. *a–d* demonstrate shape similarities and differences, whereas *e–h* show the electrostatic surfaces. pVIPR-p4α is presented identically by B*2705 and B*2709 (*d* and *h*) (5). *Red* indicates a negative surface charge, *blue* indicates a positive surface charge, and *gray areas* are uncharged.

TABLE III
pLMP2-stimulated CTL and assessment of pLMP2/pVIPR cross-reactivity

Donor[a]	Tested on B*2705·pLMP2	Tested on B*2709·pLMP2	Tested on B*2705·pVIPR	Tested on B*2709·pVIPR
CV	4/4[b]	4/4	0/4	0/4
MP	4/4	4/4	2/4	2/4
MA	3/3	3/3	0/3	0/3
BO	1/1	1/1	0/1	0/1
EP	4/4	4/4	0/4	0/4
Ci	9/9	9/9	1/4, 5 NT[c]	2/9

[a] Donor CV is a healthy *HLA-B*2705*-positive individual. Donors MP, MA, BO, and EP are *HLA-B*2705*-positive patients with AS, and donor Ci is an *HLA-B*2709*-positive healthy individual.
[b] No. of CTL with positive reactivity/total no. of CTL tested.
[c] NT, not tested.

the pVIPR peptide (pLys^{3}Arg) 32 can lead to considerable alterations in the reactivity of CTL lines (Table V). pVIPR-pArg^3 abolishes or diminishes the reactivity of the majority of the pVIPR-specific CTL. Lack of reactivity is unlikely to be influenced by the fact that oligoclonal CTL lines were used in the studies reported here, because their oligoclonality would be expected to enhance and not to diminish their cross-reactive potential. Only two CTL (AB4 and AB5) were found that re-

TABLE IV
pVIPR-stimulated CTL and assessment of pVIPR/pLMP2 cross-reactivity (only pVIPR-stimulated, pLMP2-cross-reactive CTL are shown)

CTL[a]	Tested on B*2705·pVIPR	Tested on B*2709·pVIPR	Tested on B*2705·pLMP2	Tested on B*2709·pLMP2
MP 70	48[b]	33	39	47
AS 38	68	63	38	27
AB 5	60	51	41	33
MP VPAC 7	42	45	64	41
MP VPAC 22	52	50	78	62
EP VIP 37	67	62	20	31

[a] All donors are *HLA-B*2705*-positive AS patients.
[b] Percentage of specific lysis of T2-B*2705 or T2-B*2709 cells after background subtraction.

TABLE V
pVIPR-stimulated CTL and assessment of pVIPR/pVIPR-pArg^3 cross-reactivity

CTL[a]	Tested on B*2705·pVIPR	Tested on B*2709·pVIPR	Tested on B*2705·pVIPR-pArg^3	Tested on B*2709·pVIPR-pArg^3
EP 76	41[b]	4	13	7
LV 72	73	57	3	6
PM 65	54	80	4	NT[c]
PM 46	44	48	9	7
PM 45	47	63	13	NT
MP VPAC 7	57	51	23	11
PM 53	68	63	28	36
LV 1	58	55	28	NT
AB 4	42	52	49	NT
AB 5	60	51	59	NT
PM 63	75	62	10	77

[a] All donors are *HLA-B*2705*-positive AS patients except LV who is an *HLA-B*2702*-positive AS patient.
[b] Percentage of specific lysis of T2-B*2705 or T2-B*2709 cells after background subtraction.
[c] NT, not tested.

tained their level of pVIPR-directed reactivity also with pVIPR-pArg^3 (B*2709 not tested), and two others (PM53 and LV1) had reduced activity (B*2702-derived LV1 not tested on B*2709). A single CTL (PM 63) reacted with pVIPR-pArg^3 only in the context of B*2709, although pVIPR was recognized when presented by both subtypes.

DISCUSSION

The results presented here show that a pathogen-derived peptide such as pLMP2 can exhibit MHC class I subtype-dependent, drastically distinct binding modes (Fig. 1). Although pLMP2 is not an immunodominant peptide for HLA-B*2705 (32), specific CTL are readily detectable in individuals with this subtype (4), and cross-reactivity between B*2705 and B*2709 presenting this peptide is invariably observed (Tables III, IV, and V), most likely because of the existence of nearly identical structures around the N- or C-terminal regions of the complexes (p1–p3 and p8–p9; Figs. 2 and 3 and Table II). Under natural conditions, CTL cross-reactivity between the subtypes will be experienced only very rarely; because the B*2709 subtype is found exclusively among Sardinians (1, 2), one can calculate that there are currently only about 100 living *B*2705/B*2709* heterozygous individuals (the frequency of the two subtypes in Sardinia is about 1.6 and 0.4%, respectively (2, 33). On the other hand, the worldwide distribution of the *B*2705* allele (1) and the very frequent development of immune responses against EBV (34, 35) indicate that cross-reactivity between the pLMP2 and pVIPR peptides in the context of B*2705 might be much more frequent.

Do the structural findings obtained at 100 K correlate with pLMP2/pVIPR CTL cross-reactivity assessed at 37 °C in the context of HLA-B27? It is principally possible that pLMP2 and also pVIPR exhibit conformations at physiological temperature that are not identical to those found in the crystals grown at 18 °C. However, we regard this as extremely unlikely because until now no case has been reported to our knowledge where a crystal structure suffered significant changes when diffraction data were collected at ambient and 100 K temperatures (36, 37). Similarly, the folding of the polypeptide chains in protein structures determined in solution by NMR and in the crystalline state by x-ray diffraction are comparable as are the conformations of side chains in the protein interior (38–40). Differences have been observed with side chains at the periphery that are engaged in crystal contacts, and significant differences have been reported in selected cases, *e.g.* for the inflammatory protein C3a and interleukin 8 (38). The issue of structural identity or similarity at different temperatures and states could eventually be resolved with dynamical studies of these molecules at physiological temperature (41) that must be conducted *in vitro*. Consequently, purists could again raise questions concerning the behavior *in vivo*. We have, however, taken great care that the peptides were present during the cytotoxicity tests only in HLA-B27-bound form by washing the target cells before exposure to CTL. This should favor the exclusive presence of the thermodynamically most advantageous conformation, which is very probably that or very close to that observed in the crystals.

Because the peptides exhibit sequence dissimilarity from p7 to p9 (neglecting the conservative exchange pArg^3/pLys^3) associated with differences in shape and charge distribution (Fig. 3), it seems likely that the N-terminal halves of the peptides give rise to functional and structural mimicry. Remarkably, only one of the two pVIPR conformations (p6α) shows extensive structural mimicry with pLMP2 (Figs. 2 and 3). Here, structural equivalence extends at least from residues p1 to p6 and might even include the area above residue p7. Functional molecular mimicry in B*2705, *i.e.* CTL cross-reactivity between pLMP2 and pVIPR, could be facilitated also by the higher flexibility exhibited by pLMP2 when bound to this subtype as compared with B*2709 (Fig. 1).

In contrast, cross-reactivity between the conformations of pLMP2 (p6α binding mode) and pVIPR-p4α seems much less likely (Figs. 2 and 3). Not only the overall shapes of the two structures are distinct, but the electrostatic surfaces exhibit considerable dissimilarity as well. Only the surfaces around

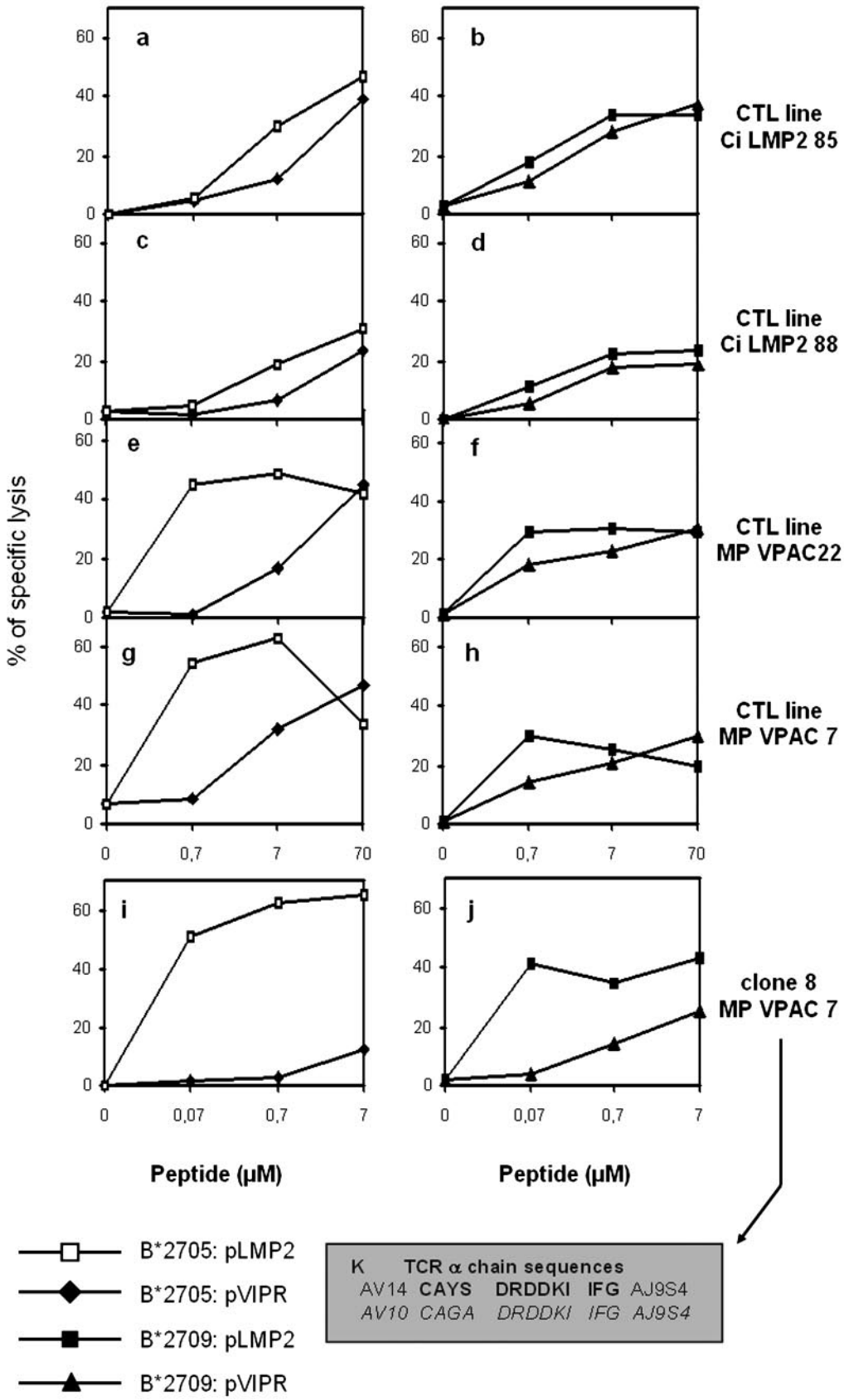

FIG. 4. **Comparison of the lytic potential of pLMP2/pVIPR-cross-reactive CTL.** Dose-response curves (effector:target ratio, 15:1) show the cytotoxic activity of four pLMP2-stimulated (*a–d*) or pVIPR-stimulated (*e–h*) CTL lines against T2-B*2705 (*a*, *c*, *e*, and *g*) or T2-B*2709 (*b*, *d*, *f*, and *h*) cells pulsed with pLMP2 or pVIPR at different concentrations. *i* and *j* show the dose-response curves of the cytotoxic activity (effector:target ratio, 3:1) of a representative clone (clone 8) derived from the CTL line MP VPAC 7. The spontaneous release of ^{51}Cr-labeled cells was less than 15%. One of three separate experiments is shown. The sequence of the TCRα-chain expressed by clone 8 (*k*, *upper line*, in *bold*) as well as that of cross-reactive clones (*k*, *lower line*, in *italics*) with specificity for peptides derived from the BZLF1 protein of EBV and a serine/threonine kinase (see text) (34) are also depicted.

the residues p1–p3 are very similar. The reactivities of pVIPR-specific CTL with pVIPR- or pVIPR-pArg^3-loaded B*2705 molecules corroborate these conclusions (Tables III, IV, and V). They show that the majority of CTL is negatively influenced by the pLys^{3}Arg replacement, suggesting that the epitopes of their TCR encompass the area around this residue. TCR α-chain-binding footprints are generally located above the N-terminal half of the peptides and the surrounding binding groove residues (42–46). Therefore, an involvement of the N-terminal half of the pLMP2 and pVIPR peptides as putative TCR epitopes suggests that TCR α-chains may contribute to the recognition process.

This assumption is supported by our finding that CTL clones derived from the MP VPAC 7 line use the same TCR α-chain CDR3 and J-region motifs as clones shown to recognize two peptides derived from a viral (BZLF1 protein of EBV, RAKFKQLL) and a self-protein (serine/threonine kinase, RSKFRQIV) (34) (Fig. 4). These otherwise completely unrelated CTL clones (HLA-B27- or HLA-B8-restricted, respectively) each recognize peptides with pArg^1. It appears therefore plausible that charge complementarity between pArg^1 and aspartic acid residues in the TCR α-chain CDR3 regions of both types of CTL could be crucial to the recognition process, supporting our assumption of the particular relevance of the N-terminal half of the peptides in pLMP2/pVIPR functional and structural mimicry. However, it is currently unknown whether a relationship exists between the observed cross-reactivity of the two HLA-B27-presented peptides, the development of differential T cell repertoires in the two subtypes, and AS pathogenesis. It even remains possible that pLMP2 and pVIPR are not the peptides that exhibit molecular mimicry relevant in the context of AS but other, possibly heteroclitic, peptides that exhibit cross-reactivity with the former. Nevertheless, these two peptides allow elucidation of the structural basis of TCR cross-reactivity in HLA-B27 subtypes that are differentially associated with an autoimmune disease (1–4).

MHC class II molecules are more likely to generate examples of structural mimicry of T cell epitopes than class I antigens (8, 9), because peptides are anchored not only at the termini but also at several positions along an MHC class II binding groove. This allows the formation of highly similar TCR epitopes even when distantly related peptides are presented by different HLA class II molecules (9). However, functional molecular mimicry has already been shown for MHC class I antigens in mice and humans, and EBV-specific memory T cell clones recognizing cross-reactive self-peptides have been found in the periphery (34) and even in joints (47). Our results complement functional data (4, 5, 34, 47) by providing a structural basis for CTL cross-reactivity also for class I molecules, with the pLMP2 and pVIPR peptides presented by HLA-B27 antigens as paradigms. These results suggest that cellular mechanisms underlying disease association with HLA class I antigens may not be fundamentally different from those observed with HLA class II molecules.

The four criteria required for a clear-cut case of molecular mimicry as a cause for autoimmunity (48) are only partially fulfilled in the context of *HLA-B27*. There is evidence for T cells directed against a self-antigen (pVIPR) nearly exclusively in individuals with the AS-associated subtype (4), and a viral mimic (pLMP2) of this self-antigen has been identified (Ref. 4 and this study). On the other hand, although the presence of EBV-specific and self-cross-reactive CTL has been demonstrated in the periphery and joints, for example in patients with oligoarticular juvenile idiopathic arthritis (49), an epidemiological association between AS and EBV has not been found so far and is hard to demonstrate given the fact that about 90% of humans get this infection during the first decades of life (35). Furthermore, no animal models are available involving presentation of pVIPR and pLMP2 in the context of HLA-B27. It is currently unknown whether the structural mimicry described here and the functional dichotomy between B*2705 and B*2709 extend to *HLA-B27* subtypes such as *B*2704* and *B*2706*, which are differentially associated with AS as well (1).

Our findings might be relevant not only in the context of autoimmune diseases but are likely to influence also our understanding of conditions leading to acceptance or rejection of transplants (50), in particular bone marrow grafts from unrelated donors (51). In addition, polymorphism of HC residue 116 has already been shown to exert an influence on the progression to AIDS among HIV-1$^+$ patients with different HLA-B35 subtypes; alleles with a Ser^{116} (B*3501 and B*3508) were associated with slow progression, whereas B*3503 (Phe^{116} but otherwise identical to B*3501) was associated with more rapid progression (52). This difference has been suggested to be due to differential binding of HIV-derived peptides by these subtypes (52).

Structural data comparing the B*3501/B*3503 pair are not available, but a direct effect of residue 116 polymorphism on the repertoire of bound peptides through interaction with the C-terminal peptide side chain (3, 53, 54) or even with an amino acid within the middle of a peptide such as pVIPR (5) or pLMP2 (this study) has been demonstrated. Furthermore, the peptide repertoire may also be influenced indirectly by residue 116 polymorphism. This can be achieved through differential dependence on the chaperone tapasin for loading of peptide cargo (54–59). For example, B*4405 can be relatively efficiently loaded with peptides also in the absence of tapasin, whereas B*4402 (differing from B*4405 only in residue 116) exhibits a complete dependence on this chaperone (54). The surface expression of tapasin-dependent HLA class I alleles may be drastically impaired, with obvious consequences for the immune response, when tapasin function is inhibited, as by the viral US3 protein following an infection with cytomegalovirus (59). Although as yet unproven, it remains a distinct possibility that B*2705 and B*2709 also exhibit differential tapasin dependence (60). In conclusion, residue 116-dependent differential peptide presentation and the ensuing distinct CTL responses could well serve to explain several of the HLA class I subtype-dependent immune phenomena observed in AS as well as in the other disease states mentioned above.

Acknowledgments—We thank all patients and healthy probands for participation in this study and are grateful to Dr. U. Müller for help with x-ray data collection at BESSY II.

REFERENCES

1. Ramos, M., and López de Castro, J. A. (2002) *Tissue Antigens* **60,** 191–205
2. D'Amato, M., Fiorillo, M. T., Carcassi, C., Mathieu, A., Zuccarelli, A., Bitti, P. P., Tosi, R., and Sorrentino, R. (1995) *Eur. J. Immunol.* **25,** 3199–3201
3. Ramos, M., Paradela, A., Vazquez, M., Marina, A., Vazquez, J., and López de Castro, J. A. (2002) *J. Biol. Chem.* **277,** 28749–28756
4. Fiorillo, M. T., Maragno, M., Butler, R., Dupuis, M. L., and Sorrentino, R. (2000) *J. Clin. Invest.* **106,** 47–53
5. Hülsmeyer, M., Fiorillo, M. T., Bettosini, F., Sorrentino, R., Saenger, W., Ziegler, A., and Uchanska-Ziegler, B. (2004) *J. Exp. Med.* **199,** 271–281
6. Oldstone, M. B. (1987) *Cell* **50,** 819–820
7. Benjamin, R., and Parham, P. (1990) *Immunol. Today* **11,** 137–142
8. Wucherpfennig, K. W. (2001) *J. Autoimmun.* **16,** 293–302
9. Lang, H. L., Jacobsen, H., Ikemizu, S., Andersson, C., Harlos, K., Madsen, L., Hjorth, P., Sondergaard, L., Svejgaard, A., Wucherpfennig, K., Stuart, D. I., Bell, J. I., Jones, E. Y., and Fugger, L. (2002) *Nat. Immunol.* **3,** 940–943
10. Geczy, A. F., and Yap, J. (1982) *J. Rheumatol.* **9,** 97–100
11. Schwimmbeck, P. L., Yu, D. T., and Oldstone, M. B. (1987) *J. Exp. Med.* **166,** 173–181
12. Ramos, M., Alvarez, I., Sesma, L., Logean, A., Rognan, D., and López de Castro, J. A. (2002) *J. Biol. Chem.* **277,** 37573–37581
13. Tiwana, H., Walmsley, R. S., Wilson, C., Yiannakou, J. Y., Ciclitira, P. J., Wakefield, A. J., and Ebringer, A. (1998) *Br. J. Rheumatol.* **37,** 525–531
14. Stone, M. A., Payne, U., Schentag, C., Rahman, P., Pacheco-Tena, C., and Inman, R. D. (2004) *Rheumatology* **43,** 148–155
15. Wucherpfennig, K. W., and Strominger, J. L. (1995) *Cell* **80,** 695–705

16. Lombardi, G., Germain, C., Uren, J., Fiorillo, M. T., du Bois, R. M., Jones-Williams, W., Saltini, C., Sorrentino, R., and Lechler, R. (2001) *J. Immunol.* **166,** 3549–3555
17. Kalams, S. A., Johnson, R. P., Trocha, A. K., Dynan, M. J., Ngo, H. S., D'Aquila, R. T., Kurnick, J. T., and Walker, B. D. (1994) *J. Exp. Med.* **179,** 1261–1271
18. Otwinowski, Z., and Minor, W. (1997) *Methods Enzymol.* **276,** 307–326
19. Collaborative Computational Project Number 4 (1994) *Acta Crystallogr. Sect. D Biol. Crystallogr.* **50,** 760–763
20. Brünger, A. T., Adams, P. D., Clore, G. M., DeLano, W. L., Gros, P., Grosse-Kunstleve, R. W., Jiang, J. S., Kuszewski, J., Nilges, M., Pannu, N. S., Read, R. J., Rice, L. M., Simonson, T., and Warren, G. L. (1998) *Acta Crystallogr. Sect. D Biol. Crystallogr.* **54,** 905–921
21. Murshudov, G. N., Vagin, A. A., Lebedev, A., Wilson, K. S., and Dodson, E. J. (1999) *Acta Crystallogr. Sect. D Biol. Crystallogr.* **55,** 247–255
22. Jones, T. A., and Kjeldgaard, M. (1997) *Methods Enzymol.* **277,** 173–208
23. Perrakis, A., Morris, R., and Lamzin, V.S. (1999) *Nat. Struct. Biol.* **6,** 458–463
24. Winn, M. D., Isupov, M. N., and Murshudov, G. N. (2001) *Acta Crystallogr. Sect. D Biol. Crystallogr.* **57,** 122–133
25. Merritt, E. A. (1999) *Acta Crystallogr. Sect. D Biol. Crystallogr.* **55,** 1109–1117
26. Hooft, R. W., Vriend, G., Sander, C., and Abola, E. E. (1996) *Nature* **381,** 272
27. Nicholls, A., Sharp, K. A., and Honig, B. (1991) *Proteins* **11,** 281–296
28. Kraulis, P. J. (1991) *J. Appl. Crystallogr.* **24,** 946–950
29. Sanner, M. F., Olson, A. J., and Spehner, J. C. (1996) *Biopolymers* **38,** 305–320
30. Merritt, E. A., and Bacon, D. J. (1997) *Methods Enzymol.* **277,** 505–527
31. Madden, D. R. (1995) *Annu. Rev. Immunol.* **13,** 587–622
32. Brooks, J. M., Murray, R. J., Thomas, W. A., Kurilla, M. G., and Rickinson, A. B. (1993) *J. Exp. Med.* **178,** 879–887
33. Contu, L., Arras, M., Carcassi, C., La Nasa, G., and Mulargia, M. (1992) *Tissue Antigens* **40,** 165–174
34. Misko, I. S., Cross, S. M., Khanna, R., Elliott, S. L., Schmidt, C., Pye, S. J., and Silins, S. L. (1999) *Proc. Natl. Acad. Sci. U. S. A.* **96,** 2279–2284
35. Moss, D. J., Burrows, S. R., Silins, S. L., Misko, I., and Khanna, R. (2001) *Philos. Trans. R. Soc. Lond. B Biol. Sci.* **356,** 475–488
36. Earnest, T., Fauman, E., Craik, C. S., and Stroud, R. (1991) *Proteins* **10,** 171–187
37. Tilton, R. F., Dewan, J. C., and Petsko, G. A. (1992) *Biochemistry* **31,** 2469–2481
38. Wagner, G., Hyberts, S. G., and Havel, T. F. (1992) *Annu. Rev. Biophys. Biomol. Struct.* **21,** 167–198
39. Stollar, E. J., Mayor, U., Lovell, S. C., Federici, L., Freund, S. M. V., Fersht, A. R., and Luisi, B. F. (2003) *J. Biol. Chem.* **278,** 43699–43708
40. Liu, Y., Zhang, X., Yoshida, T., and La Mar, G. N. (2004) *Biochemistry* **43,** 10112–10126
41. Pöhlmann, T., Böckmann, R. A., Grubmüller, H., Uchanska-Ziegler, B., Ziegler, A, and Alexiev U. (2004) *J. Biol. Chem.* **279,** 28197–28201
42. Garboczi, D. N., Ghosh, P., Utz, U., Fan, Q. R., Biddison, W. E., and Wiley, D. C. (1996) *Nature* **384,** 134–141
43. Garcia, K. C., Degano, M., Stanfield, R. L., Brunmark, A., Jackson, M. R., Peterson, P. A., Teyton, L., and Wilson, I. A. (1996) *Science* **274,** 209–219
44. Reiser, J. B., Darnault, C., Guimezanes, A., Gregoire, C., Mosser, T., Schmitt-Verhulst, A. M., Fontecilla-Camps, J. C., Malissen, B., Housset, D., and Mazza, G. (2000) *Nat. Immunol.* **1,** 291–297
45. Housset, D., and Malissen, B. (2003) *Trends Immunol.* **24,** 429–437
46. Kjer-Nielsen, L., Clements, C. S., Purcell, A. W., Brooks, A. G., Whisstock, J. C., Burrows, S. R., McCluskey, J., and Rossjohn, J. (2003) *Immunity* **18,** 53–64
47. Selin, L. K., and Welsh, R. M. (2004) *Immunity* **20,** 5–16
48. Rose, N. R., and Bona, C. (1993) *Immunol. Today* **14,** 426–430
49. Massa, M., Mazzoli, F., Pignatti, P., De Benedetti, F., Passalia, M., Viola, S., Samodal, R., La Cava, A., Giannoni, F., Ollier, W., Martini, A., and Albani, S. (2002) *Arthritis Rheum.* **46,** 2721–2729
50. Doxiadis, I. I., Smits, J. M., Schreuder, G. M., Persijn, G. G., van Houwelingen, H. C., van Rood, J. J., and Claas, F. H. (1996) *Lancet* **348,** 850–853
51. Ferrara, G. B., Bacigalupo, A., Lamparelli, T., Lanino, E., Delfino, L., Morabito, A., Parodi, A. M., Pera, C., Pozzi, S., Sormani, M. P., Bruzzi, P., Bordo, D., Bolognesi, M., Bandini, G., Bontadini, A., Barbanti, M., and Frumento, G. (2001) *Blood* **98,** 3150–3155
52. Gao, X., Nelson, G. W., Karacki, P., Martin, M. P., Phair, J., Kaslow, R., Goedert, J. J., Buchbinder, S., Hoots, K., Vlahov, D., O'Brien, S. J., and Carrington, M. (2001) *N. Engl. J. Med.* **344,** 1668–1675
53. Hülsmeyer, M., Hillig, R. C., Volz, A., Rühl, M., Schröder, W., Saenger, W., Ziegler, A., and Uchanska-Ziegler, B. (2002) *J. Biol. Chem.* **277,** 47844–47853
54. Zernich, D., Purcell, A. W., Macdonald, W. A., Kjer-Nielsen, L., Ely, L. K., Laham, N., Crockford, T., Mifsud, N. A., Bharadwaj, M., Chang, L., Tait, B. D., Holdsworth, R., Brooks, A. G., Bottomley, S. P., Beddoe, T., Peh, C. A., Rossjohn, J., and McCluskey, J. (2004) *J. Exp. Med.* **200,** 13–24
55. Peh, C. A., Burrows, S. R., Barnden, M., Khanna, R., Cresswell, P., Moss, D. J., and McCluskey, J. (1998) *Immunity* **8,** 531–542
56. Turnquist, H. R., Thomas, H. J., Prilliman, K. R., Lutz, C. T., Hildebrand, W. H., and Solheim, J. C. (2000) *Eur. J. Immunol.* **30,** 3021–3028
57. Turnquist, H., Schenk, E. L., McIlhaney, M. M., Hickman, H. D., Hildebrand, W. H., and Solheim, J. C. (2002) *Immunogenetics* **53,** 830–834
58. Hildebrand, W. H., Turnquist, H. R., Prilliman, K. R., Hickman, H. D., Schenk, E. L., McIlhaney, M. M., and Solheim, J. C. (2002) *Hum. Immunol.* **63,** 248–255
59. Park, B., Kim, Y., Shin, J., Lee, S., Cho, K., Fruh, K., Lee, S., and Ahn, K. (2004) *Immunity* **20,** 71–85
60. Uchanska-Ziegler, B., Alexiev, U., Hillig, R., Hülsmeyer, M., Pöhlmann, T., Saenger, W., Volz, A., and Ziegler, A. (2004) in *Proceedings of the 13th International Histocompatibility Workshop and Congress* (Hansen, J.A., and Dupont, B., eds) International Histocompatibility Working Group Press, Seattle, in press

Allele-dependent Similarity between Viral and Self-peptide Presentation by HLA-B27 Subtypes

Maria Teresa Fiorillo, Christine Rückert, Martin Hülsmeyer, Rosa Sorrentino, Wolfram Saenger, Andreas Ziegler and Barbara Uchanska-Ziegler

J. Biol. Chem. 2005, 280:2962-2971.
doi: 10.1074/jbc.M410807200 originally published online November 10, 2004
